Aerosol Science and Technology
Publication details, including instructions for authors and subscription information:
http://www.tandfonline.com/loi/uast20

Numerical Simulations on Aerodynamic Focusing of Particles in a Wide Size Range of 30 nm-10 μm

Kwang-Sung Lee [a] , Tae-Hyun Hwang [a] , Seok-Hwan Kim [a] , Soo Hyung Kim [b] & Donggeun Lee [a]

[a] School of Mechanical Engineering, College of Engineering , Pusan National University , Busan , South Korea

[b] Department of Nanomechatronics Engineering, College of Nanoscience and Nanotechnology , Pusan National University , Busan , South Korea

Accepted author version posted online: 29 May 2013.Published online: 18 Jun 2013.

To cite this article: Kwang-Sung Lee , Tae-Hyun Hwang , Seok-Hwan Kim , Soo Hyung Kim & Donggeun Lee (2013): Numerical Simulations on Aerodynamic Focusing of Particles in a Wide Size Range of 30 nm-10 μm, Aerosol Science and Technology, 47:9, 1001-1008

To link to this article: http://dx.doi.org/10.1080/02786826.2013.808737

Aerosol Science and Technology, 47:1001–1008, 2013

ISSN: 0278-6826 print / 1521-7388 online
DOI: 10.1080/02786826.2013.808737

Numerical Simulations on Aerodynamic Focusing of Particles in a Wide Size Range of 30 nm–10 μm

Kwang-Sung Lee,[1] Tae-Hyun Hwang,[1] Seok-Hwan Kim,[1] Soo Hyung Kim,[2] and Donggeun Lee[1]

[1]*School of Mechanical Engineering, College of Engineering, Pusan National University, Busan, South Korea*

[2]*Department of Nanomechatronics Engineering, College of Nanoscience and Nanotechnology, Pusan National University, Busan, South Korea*

Previous designs of conventional aerodynamic lenses have the limitation of a narrow range of focusable particle size, e.g., just one order of magnitude such as 30–300 nm or 3–30 nm. To enlarge the focusable size range to two orders of magnitude (30–3,000 nm), it is necessary to focus small particles and at the same time not to loose the large ones. From numerical simulations of size-resolved particle trajectories, we confirmed that the traveling losses of such large particles could be avoided only when the radial positions of particles approaching the orifice lenses were near the axes of the lenses. Hence, we designed a lens system consisting of seven orifices to fulfill the requirement. In particular, the orifices were aligned in such a way that their diameters would descend and ascend downstream. As a result, 30–2500 nm particles could be focused to produce particle beams with radii of 0.2 mm or less with a transmission efficiency of above 90% 40 mm downstream of the aerodynamic lens exit. Even 10 μm particles could be focused with a transmission efficiency of 80%.

1. INTRODUCTION

Consisting of multi-stage orifices, aerodynamic lenses are devices that generate aerosol particle beams by focusing nanosized particles with a high transmission efficiency. First proposed by Liu et al. (1995a,b), they have the advantage of being mechanical devices that can be manufactured easily without special electric control units. Submicron particle focusing technology using aerodynamic lenses has diverse applications, including effective aerosol inlets for aerosol mass spectrometers (Schreiner et al. 1999; Jayne et al. 2000; Zhang et al. 2004; Lee et al. 2005, 2006, 2008; Liu et al., 2007), micropatterning and material synthesis (Fonzo et al. 2000; Dong et al. 2004; Qi et al. 2010), and inlets for measuring the creation of biomaterials (Harris et al. 2006).

Although aerosol particle beams can be generated by various tools, including capillary tubes (Murphy and Sears 1964), orifices (Das and Phares 2004; Deng et al. 2008), or converging nozzles (Chen and Pui 1995), the application of each particle beam-generating tool is very limited due to narrow window for their size classification capacity. Created by inserting 3–5 planar orifices with disparate inner diameters in a cylindrical tube at appropriate intervals, aerodynamic lenses are able to focus a far broader size range of submicron particles with high transmission efficiency (Liu et al. 1995a,b). With most aerodynamic lens designs proposed to date, however, only particles in a range of one order of magnitude in diameter can be focused: 25–250 nm for Liu et al. (1995a,b), 100–900 nm for Schreiner et al. (1998), 340–4000 nm for Schreiner et al. (1999), 60–600 nm for Zhang et al. (2004), 3–30 nm for Wang et al. (2005), 30–300 nm for Lee et al. (2008), and 5–50 nm for Lee et al. (2009).

Hence, in the case of the Series 3800 ATOFMS model manufactured by TSI, two aerodynamic lens models must be replaced to conduct mass analysis on aerosol particles of 30 nm−3 μm (TSI, 2004). This signifies a serious problem where particles with wide-range sizes cannot be subjected to mass analysis all at once and considerable time is necessary to satisfy actual-use conditions after replacing the aerodynamic lenses because aerosol mass spectrometry by nature requires a high-vacuum state.

It is known that disparate phenomena characterize upper and lower limits in such focusable particle size ranges. First, in the case of lower limits, or when the particles to be focused are

Received 4 February 2013; accepted 27 April 2013.

This work was supported by the National Research Foundation of Korea (NRF) grants funded by the Korean government (MEST) (No. 2012-0008830). The authors also appreciate the financial support from "Development of the Preparation Technology of 0.1–10 μm Sized Metal Powders and Fine-Components for Micro Electronics" of Ministry of Knowledge Economy (MKE) and Korea Research Council for Industrial Science and Technology (ISTK) of the Republic of Korea.

Address correspondence to Donggeun Lee, School of Mechanical Engineering, College of Engineering, Pusan National University, 30 Jangjeon-dong, Geumjeong-gu, Busan 609-735, South Korea. E-mail: donglee@pusan.ac.kr

very small, measuring 30 nm or less, not only is the inertia of particles insufficient for focusing the particles, but also the particles readily diverge due to diffusion, thus making it difficult to focus. To overcome such difficulties, methods including the use of helium instead of air as the carrier gas (Wang et al. 2005) or the change of the aerodynamic lenses' geometrical shapes to converging-diverging types (Lee et al. 2009) were recently proposed. On the contrary, the upper limit of the ranges is generally restricted due to the excessive inertia of large particles. In other words, if the particle Stokes number (St) is 10 or above, it can lead to a dramatic increase in transmission loss caused by the inertial impact of large particles. However, the loss of such large particles has not been carefully taken into consideration in lens designs, nor are there known reports on ways to resolve the problem. Because enlarging the upper limits is more efficient to expand the focusable-particle size range of the lens, the present study is focused on the behavior and loss prevention of particles with large St (i.e., St $>$ 10). It is worth noting that Schreiner et al.'s (1999) 7-stage aerodynamic lens is the only design that has been experimentally demonstrated to focus micron particles, but designing concept was not clearly stated.

Within aerodynamic lenses, particles with large St are subjected to collision loss in front of the orifices or, after being overfocused in the orifices, subjected to collision loss on the spacer or the orifices at the next stage. In addition, as particles approach an orifice, the local St (Liu et al. 1995a; Wang & McMurry 2006; Deng et al. 2008) varies with radial positions, mainly due to disparity in the particle velocity, so that the particle collision loss becomes highly dependent on their radial positions upstream the orifice. Consequently, in the present study, the orifices were arranged in two stages (with the orifice diameters increasing after decreasing first). In the first stage, the incidence position of large particles was made to move close to the central axes of the lenses and, in the second stage, the divergence angles of particles were reduced to minimize further inertial impaction. The design goal was established as focusing particles with wide-range diameters of 30 nm–10 μm with minimal loss and was confirmed through numerical analysis. However, it has to be clarified that the present design was focused on the aerodynamic lens alone excluding the critical orifice where micron particles are often lost significantly.

2. SIMULATION FOR TRACING NANO- AND MICROPARTICLES

As for the simulation of the flow of air and the behavior of the particles within aerodynamic lenses, FLUENT (version 6.2.16) was used. Because the number concentration of particles was low and particle diameters were small relative to mean free path of gas at low pressure, the particles were hypothesized not to affect the air flow and interaction among them was neglected. The flow rate of the inlet air was limited to 100 sccm (2.04×10^{-6} kg/s) by a critical orifice with a diameter of 0.1 mm so that the pressure at the inlet was maintained at $\sim$80 Pa (1.36 torr). The pressure at the lens outlet was hypothesized to be $\sim$0.13 Pa (10^{-3} torr), which is the operating condition of aerosol mass spectrometers (Lee et al. 2005, 2006, 2008). In addition, the fluid flow was hypothesized to be a steady state, compressible, axisymmetric, laminar, and viscous flow (Lee et al. 2008; Wang et al. 2005; Zhang et al. 2004). The Fluent's preprocessor Gambit was used to create the quadrilateral mesh of approximately 130,000 cells with 0.25×0.25 mm^2. The particles were hypothesized to be spherical and have the unit density ($\rho_p = 1$ g/cc). Because the slip correction factor changes according to the gas pressure, the user-defined function (UDF) was used to prompt it to change according to continuous changes in the pressure inside the aerodynamic lenses (Lee et al. 2009; Wang et al. 2005).

As for the behavior of particles, their trajectories were determined by the initial velocity and drag force of the particles and lift force was disregarded due to the symmetric shape of the particles. In the present study, the effect of Brownian diffusion was included in calculations of the particles of 30–300 nm. The calculations were repeated 20 times, including the average values and standard deviation (SD) values in the particle beam radii and the results of the transmission rates. The motion of the particles, including drag force and the diffusion effect, is expressed as in Equations (1)–(3):

$$\frac{du_p}{dt} = F_{\text{drag}} + F_{\text{bi}} \quad [1]$$

$$F_{\text{drag}} = \frac{u_f - u_p}{\tau} = \frac{3\pi\mu d_p(u_f - u_p)}{m_p C_c} \quad [2]$$

$$F_{\text{bi}} = G_i\sqrt{\frac{\pi S_0}{\Delta t}};\ S_o = \frac{216\nu kT}{\pi^2\rho d_p^5\left(\frac{\rho_p}{\rho}\right)^2 C_c}, \quad [3]$$

where u_p and u_f represent the velocity of particles and fluid, τ represents the relaxation time of particles, F_{drag} and F_{bi} represent drag force and Brownian force per unit mass, respectively, and drag force follows Stokes' law. ν represents the kinematic viscosity of the air, d_p represents the particle diameter, m_p represents the particle mass, C_c represents the slip correction factor, and G_i represents zero-mean, unit-variance, independent Gaussian random numbers, k represents Boltzmann constant, T represents upstream temperature, and ρ represents air density, respectively (Wang et al. 2005: Li and Ahmadi 1992). To obtain particle trajectories, numerical integration of Equation (1) was performed in Fluent with the time step size, which is implicitly set by the step length factor of 5.

The St of particles was calculated (Liu et al. 1995a; Wang et al. 2005) in accordance with the definition of Epstein's mobility as:

$$\text{St} = \frac{\tau u_0}{d_f} = \frac{\rho_p d_p^2 C_c u_0}{18\mu_0 d_f}, \quad [4]$$

where τ represents the particle relaxation time, u_0 represents average gas velocity at an orifice throat, d_f represents inner diameter of each orifice, μ_0 is gas viscosity, respectively. It is noted that the average value of gas velocity u_0 has been inevitably used for designs of the aerodynamic lens to date. However, replacing the average velocity u_0 with a real gas velocity u_f at local positions, the readers readily notice how local St in reality deviates from the St used in design and why the particle collision loss highly depends on their radial incidence positions toward an orifice as well.

3. RESULTS AND DISCUSSIONS

3.1. Aerodynamic Lens for Focusing 30 nm–10 μm Particles

Figure 1 is a drawing of aerodynamic lens system designed for focusing particles with wide-range diameters of 30 nm–10 μm. The aerodynamic lens system consists of seven orifices and a nozzle inside a cylindrical tube. The figure clearly indicates the generation of repeated converging/diverging flow pattern with orifices, which drives aerodynamic focusing (Wang & McMurry 2006). The lens system was designed in two parts. In the first part, the inner diameters of the orifices were set to gradually decrease until the 5th orifice, in a way that the St of the particles would become the maximum at the 5th orifice and the radial positions (r_{pi}) of particles measuring 30 nm–10 μm would contract gradually until $r_{pi}/R < 0.1$, where R is the inner radius of the tube. After the 5th orifice as the second part, the orifice diameters (d_f) once again increased, leading the particle St to decrease. The purpose of this part design is to minimize the inertial impact loss of particles by suppressing the divergence of the particle beams and to collimate the particle beams such that they will enter the nozzle safely. Table 1 shows the St variations of different-sized particles along the orifices per particle size and orifice lens and the St was confirmed to increase gradually up to the 5th lens, and to decrease again at the 6th–7th lenses.

In Figure 1, the inner diameter (d_f) of the 1st orifice and the tube diameter (OD) are 13 mm and 25 mm, respectively, and the ratio of the d_f to OD is 0.52. Earlier research has demonstrated that when d_f/OD > 0.4, though no optimal stokes number St_o exists at any particle diameter, wide-range of particles ($0.01 < St < 10$) can be suboptimally focused with reduced transmission

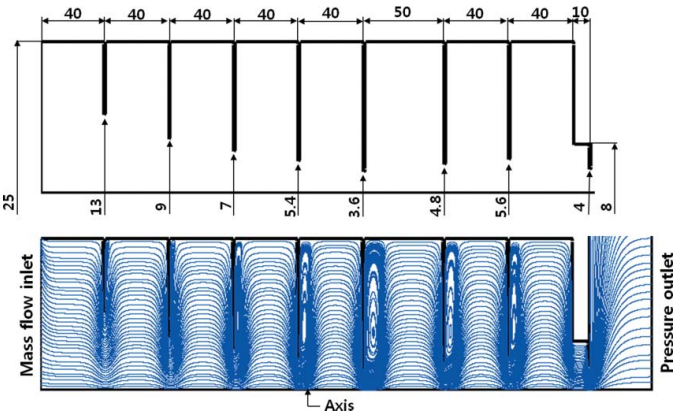

FIG. 1. Schematic of an aerodynamic lens system and gas flow streamlines at $Q = 100$ sccm; all numeric values are in units of mm. (Color figure available online.)

loss (Zhang et al. 2002). On the contrary, when d_f/OD $= 0.3$, though small particles ($St < 0.5$) can be focused, large particles ($St > 0.5$) are too much overfocused and finally lost. This must be avoided in the present study. Consequently, in the present study, the purpose of the 1st stage orifice did not lie in optimal focusing, but in safe delivery of wide-range of particles even at the expense of efficient focusing by taking d_f/OD > 0.4. When the St is large, inertial impaction loss is greater in front of the orifices for particles near the tube wall than for those near the central axes of the orifices. Deng et al. (2008) have shown that, as for particles measuring 5.5–10 μm in an orifice flow with the flow rate of 200 sccm, only those particles distributed near the tube wall of $0.66 < r_{pi}/R < 0.94$ are lost due to inertial impaction. At the beginning of this study, we tested the case of d_f/OD < 0.4 for the 1st stage orifice. The result showed that $\sim$25% of particles measuring 5–10 μm were lost in front of the 1st stage lens. Hence, the inner diameter (d_f) of the 1st orifice was set to increase to d_f/OD $= 0.52$, resulting in a reduction of the inertial impact loss of 5–10 μm particles to $\sim$10%.

Figure 2 shows the flow velocity and pressure changes of carrier gas, and the particle velocity along the central axis. Excluding the nozzle, which is responsible for acceleration, the flow velocity and pressure changes are the greatest at the 5th lens. Upon passing through the orifices, Particles of 30 nm and 300 nm, respectively, likewise accelerate and decelerate due to drag force until the particle velocity becomes almost identical

TABLE 1
Particle Stokes number (St) at each orifice

Orifice number	1	2	3	4	5	6	7
St of 30 nm particles	0.01	0.02	0.04	0.10	0.36	0.27	0.22
St of 300 nm particles	0.07	0.21	0.44	0.99	3.62	2.65	2.18
St of 1 μm particles	0.23	0.69	1.47	3.30	12.08	8.84	7.26
St of 3 μm particles	0.68	2.06	4.42	9.91	36.23	26.53	21.79
St of 10 μm particles	2.27	6.85	14.73	33.02	120.76	88.43	72.64

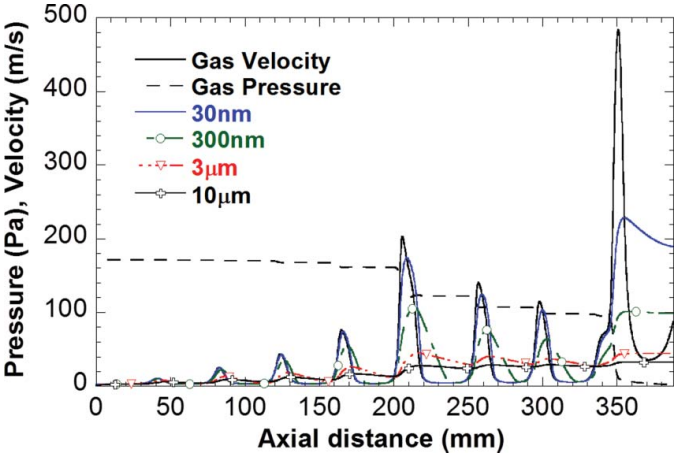

FIG. 2. Air velocity, pressure, and axial velocity of particles (d_p = 30 nm, 300 nm, 3 μm, 10 μm) along the aerodynamic lens axis. (Color figure available online.)

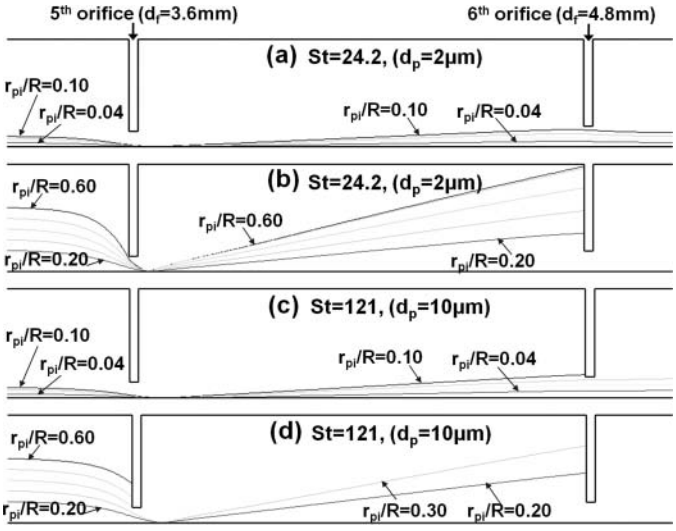

FIG. 3. St-dependent trajectories of particles approaching an orifice at various radial positions: (a and c) near the lens symmetric axis and (b and d) far from the axis.

to the flow velocity downstream of each orifice. On the contrary, particles of 3 μm and 10 μm, respectively, accelerate and decelerate relatively slowly due to large inertia and long particle relaxation time. Thus, their velocity downstream each orifice is not able to fully regress to the flow velocity, but becomes even higher than the flow velocity. This phenomenon for particles as large as 3 μm and 10 μm becomes a major factor affecting particle inertial impact and the particle divergence angle, as will be described in Section 3.2. For reference, it is confirmed that the relaxation time of particles of 30 nm between the 5th and 6th orifices (axial location: 205–255 mm) is 1.7×10^{-5} s, much shorter than those of particles measuring 3 μm and 10 μm which are 1.7×10^{-3} s and 5.8×10^{-3} s, respectively.

3.2. Inertial Impact of Particles with the St >10 and the Control of the Particle Divergence Angle

The radial positions (r_{pi}) of particles approaching an orifice greatly affect the contraction ratio and the transmission efficiency of the particles, which becomes more significant particularly when the particles of consideration are as large as several micrometers (Liu et al. 1995a). Hence, for simplicity in design, previous researchers limited either the incidence positions with respect to the outer radius of each orifice up to 0.2–0.3: $r_{pi}/R \leq$ 0.2 or 0.3 or particle sizes to submicrometer ranges. Their lens design was made on the basis of the St_0 for the particles in such a limited incidence position to be focused optimally (Lee et al. 2008; Wang and McMurry 2006).

Figure 3 clearly shows the significance of the incidence positions of particles with large St in the lens design. In Figure 3b and d, when large particles with St = 24.2 and 121 approach an orifice (indeed the 5th orifice in our design) apart from the central axis, the particles, after being overfocused at the orifice, tend to behave in a rectilinear fashion, leading to significant impaction loss. On the contrary, Figures 3a and c show if the incidence positions of those large particles are forced within the region of $r_{pi}/R \leq 0.1$, their divergence angle downstream the orifice is extremely limited, ensuring their safe journey to the next orifice. This describes the role of the 1st five orifices (1st to 5th): forcing the particle trajectories as close to the axis as possible before entering the 6th orifice.

Figure 4 is a schematic that shows how the divergence angle of particles is controlled at the 6th orifice after being overfocused: the focal point in Figure 4 denotes a point to which all particles are focused by the 5th orifice as seen in Figure 3b, and the orifice in Figure 4 corresponds to the 6th orifice in Figure 3b. As aforementioned, particles as large as several micrometers showed a linear motion after overfocused due to large inertia and long particle relaxation time, causing the divergence angle (α_{in}) to be maintained. The divergence angle of α_{in} becomes the incidence angle at the next-stage orifice and the particle trajectory would be refracted in three ways depicted in Figure 4 by the compressing gas flow. The second divergence angle after the refraction is defined as α_{out} with respect to the central axis. If the particles are so large, they are just a little refracted due to the high inertia, as noted as case (a), i.e., positive α_{out}. On the contrary, small particles readily turn their direction toward the axis, showing the case (c), i.e., negative α_{out}. Thus, there exist an adequate size of particles denoting $\alpha_{out} = 0$ (case (b)), making

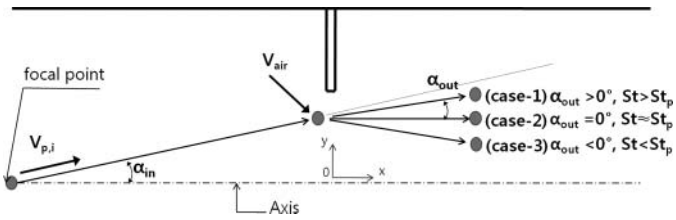

FIG. 4. Schematic diagram illustrating the variance of particle divergence angles (α_{out}) at high particle Stokes number (St > 10) in an orifice flow.

the particle trajectory parallel to the central axis. Since preventing the transmission loss of large particles is of current interest, it is a key point in design how to make the case (a) closest to the case (b). Here, the particle St (St_p) in the case (b) is considered as an optimal value in the second part of current aerodynamic lens system and the corresponding particle diameter is denoted as $d_{p,p}$.

Given the fixed values of d_f, d_f/OD, and gas flow rate Q to the 6th orifice, the divergence angles α_{out} of particles are calculated as a function of St and shown in Figure 5. In Figure 5a, the incidence angle α_{in} was fixed to 0.16°, and the three incidence velocities of particles ($V_{p,i}$ = 17.3, 24.0, and 36.7 m/s) considered here are indeed the velocities of 10, 3, and 1 μm particles, respectively, at the focal point downstream the 5th orifice. The range of St in Figure 5 corresponds to that of particle size (1–20 μm). As a result, the optimal value of St_p when α_{out} = 0° was ~17, almost invariant under changes in the incidence velocity, and the corresponding particle size $d_{p,p}$ was 1.8 μm. The angle of α_{out} denotes the largest variation around the value of St_p, from negative to positive, and gradually converges to the value of α_{in} (no refraction) as St increases. In addition, particles

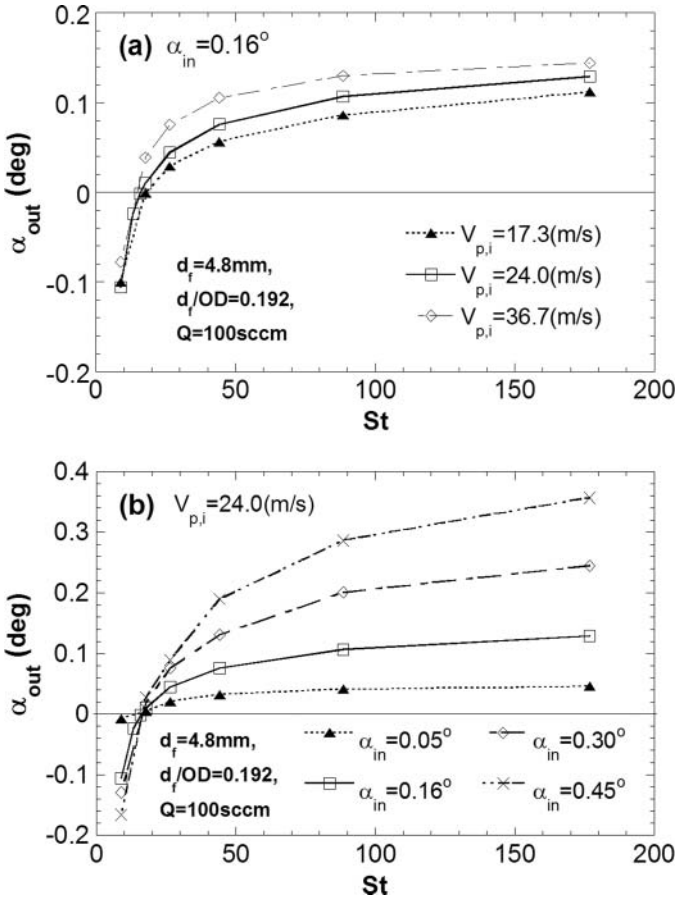

FIG. 5. Variations of the divergence angle (α_{out}) of particles: (a) with three different incidence velocities at a fixed incidence angle; (b) with a fixed incidence velocity at four incidence angles, as a function of St.

of the same size (a fixed value of St in Figure 5a) tend to diverge more, leading to an increase in the α_{out}, as their incidence velocity increases alone. The divergence depends to a large degree on the drag force component perpendicular to the lens axis (i.e., perpendicular to the general particle motion). This component of the drag force is likely not strongly affected by the particle velocity. However, with increasing particle velocity the time this force acts onto the particles decreases, potentially causing increased divergence.

In Figure 5b, the effect of the incidence angle α_{in} on the α_{out} was investigated likewise. It is interesting to note the existence of the invariant St_p, though the divergence angle α_{out} is greatly increased with increasing the incidence angle α_{in}. Another thing to note is that the smallest particles (St = 10) with an angle of $\alpha_{in} = 0.45°$ follow the case (c) in Figure 4, denoting the negative α_{out}. On the contrary, the same particles approaching with a smaller angle of $\alpha_{in} = 0.05°$ are less diverged, almost parallel to the axis (closer to the case (b)). Thus it is important to maintain the incidence angle of particles of all sizes as low as possible.

As has been stated above, the St_p of the 6th orifice for controlling the divergence angle in the present study is limited to 17 ($d_{p,p}$ = 1.8 μm). In order to raise the St_p and thereby increase $d_{p,p}$ to 5 μm or 10 μm, higher compressing gas flow at the orifice throat is required, which is realized only when the orifice diameter d_f is decreased. In this case, while there is an advantage in that degree of focusing of 5–10 μm particles becomes improved, there is another concern that, as in Figure 3, inertial impact loss of particles can be more significant on a narrowed frontal surface of the orifice and/or the next-stage orifice. For this reason, the value of St_p was adjusted to 17 in the present study.

3.3. Simulations of Particle Trajectories and Performance Evaluation of Aerodynamic Lens System

Figure 6 presents the size-resolved trajectories of particles launching at the same radial position ($r_{pi}/R = 0.5$). In Figure 6a, the first part (1st-to-5th orifices) of the lens system works so as to tightly collimate particles of all sizes to the axis, leaving the 5th orifice (at the axial distance of 205 mm) with the relative beam radius of $r_{pi}/R < 0.1$. According to Wang & McMurry (2006), the optimal value of St_0 for best focusing, which should be discriminated from the St_p, varies within the range of 0.6–1.2 depending on the Re and Ma. Taking this into consideration, the data listed in Table 1 are analyzed as follows.

The St of particles measuring 30 nm increases from 0.01 to 0.36 while the particles pass through up to the 5th orifice. The values are all smaller than the St_o, however, the St of the 5th–7th lenses amount to 0.22–0.36, high enough to make the system work suboptimally. Thus those particles gradually contract so that the particle beam radius is within 0.06 mm immediately before the particles pass through the nozzle. From Table 1, particles measuring 300 nm are expected to be optimally focused as they pass through the 4th lens. The simulation result in Figure 6a is almost identical to the expectation, leading the beam radius

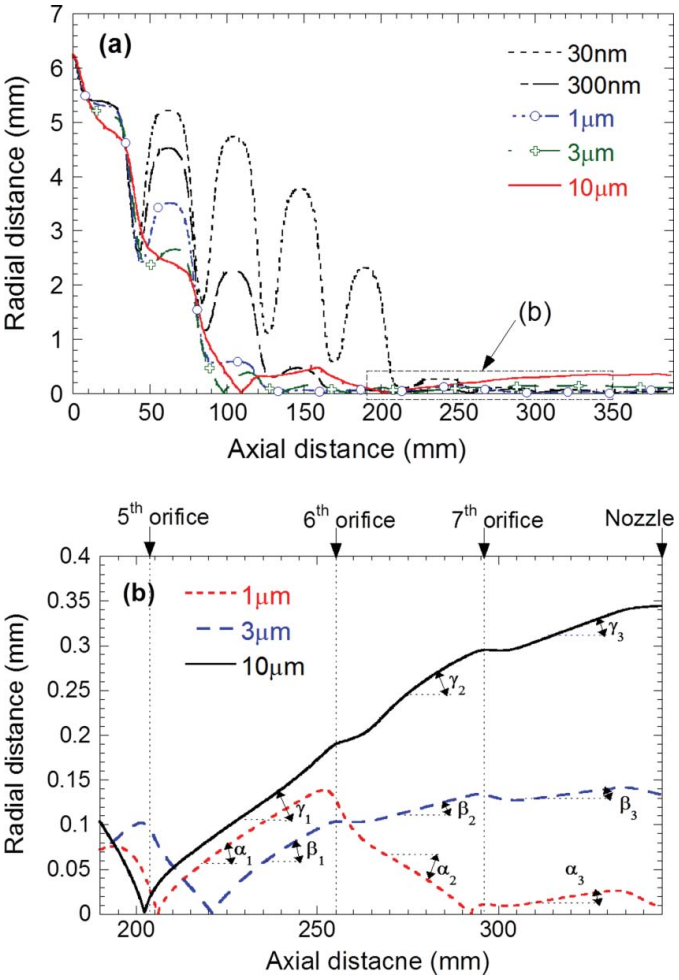

FIG. 6. (a) Size-resolved particle trajectories launched at a radial position of $r_{pi}/R = 0.5$ at an aerodynamic lens inlet; (b) particle trajectories magnified in the zone of 5th to nozzle. (Color figure available online.)

to be 0.05 mm. But, Table 1 also shows that the St increases further to the range of 2.2–3.6 at the 5th–7th orifices. According to Wang and McMurry (2006), the contraction ratio η_c was approximately -1 in the range of $2.2 < St < 3.6$ (refer to Figure 2 in their paper), implying that particles, after being overfocused, fly at the same radial distance from the axis with neither contraction nor divergence. In the end, the particle beam radius maintains its value of 0.05 mm.

Recalling that the optimal St_0 ranged from 0.6 to 1.2 (Lee et al. 2008), Table 1 indicates that the particles measuring 1 μm are optimally focused somewhere between the 2nd and 3rd orifices, while particles of 3 μm are overfocused at the 2nd orifice due to a large St. Figure 6a shows very consistent results that 1-μm particles are suboptimally focused at the 2nd orifice and then slightly overfocused at the 3rd, whereas 3-μm particles are overfocused earlier at the 2nd orifice, but still being very close to the axis ($r_{pi}/R = 0.032$) behind the 2nd orifice. As for particles measuring 10 μm, since already in the first orifice their St is larger than the St_0 (Table 1), the overfocusing is expected to occur as the particles pass through the 1st orifice and impaction loss might be inevitable. It should be, however, recalled that their results are restricted to the case of $d_f/OD < 0.4$ as discussed in Section 3.1. In the present 1st orifice, the value of d_f/OD is 0.52 in which there is neither optimal focusing nor overfocusing, so that such a significant overfocusing can be avoided and the orifices can instead work suboptimally. Overall, all particles considered here are demonstrated to be adequately focused until the 5th orifice, in a way to meet the requirement for the prevention of impaction loss of very large particles: $r_{pi}/R < 0.1$ as depicted in Figure 3.

To clarify the role of the second part of the lens system to the 1–10 μm particles, the behaviors of those particles in the region of 5th–7th orifices are magnified in Figure 6b. In the figure, the divergence angles that develop after the 1-μm particles have passed through the 5th–7th orifices are denoted as α_1, α_2, and α_3 in order. Naming the divergence angles of particles of 3 μm and 10 μm are made likewise. In addition, the divergence angles and the change ratio of divergence angles (α_{out}/α_{in}) were measured from Figure 6b and summarized in Table 2. As for 1 μm particles, since their St is 8.8 at the 6th lens (Table 1) and still smaller than St_p of 17 ($d_{p,p} = 1.8$ μm), the particles trajectory bends in a way of case (c) in Figure 4, i.e., negative α_{out}, which is clearly demonstrated in Figure 6b. Further downstream, the value of St decreases to the favorable condition for focusing, leading to less divergence of particle beam (Table 2), though the directions of the divergence angles are switched. It is noted that the change ratio of divergence angles after the particles have all passed through the 7th orifice (α_3/α_1) is only 0.25, suggesting that the divergence angle of particles leaving the 5th orifice is reduced to 1/4 so that the particles enter the nozzle with a beam radius within 0.03 mm.

TABLE 2
Particle divergence angles (α_{out}) and the change ratios of α_{out} to α_{in} according to the particle diameter and the orifice number in conjunction with Figure 6b

Particle diameter	α_{out} (deg)			Ratio of the divergence angles (α_{out}/α_{in})		
$d_p = 1$ μm	$\alpha_1 = 0.144$	$\alpha_2 = -0.158$	$\alpha_3 = 0.036$	$\alpha_2/\alpha_1 = -1.10$	$\alpha_3/\alpha_2 = -0.23$	$\alpha_3/\alpha_1 = 0.25$
$d_p = 3$ μm	$\beta_1 = 0.160$	$\beta_2 = 0.063$	$\beta_3 = 0.034$	$\beta_2/\beta_1 = 0.39$	$\beta_3/\beta_2 = 0.54$	$\beta_3/\beta_1 = 0.21$
$d_p = 10$ μm	$\gamma_1 = 0.194$	$\gamma_2 = 0.138$	$\gamma_3 = 0.117$	$\gamma_2/\gamma_1 = 0.71$	$\gamma_3/\gamma_2 = 0.85$	$\gamma_3/\gamma_1 = 0.60$

On the contrary, Table 1 indicates that particles as large as 3 μm or 10 μm all have the St greater than the St_p of 17 at the 6th and 7th orifices. Thus, the particle trajectories develop in the path of case (a) in Figure 4, i.e., positive α_{out}. As for 3-μm particles, because the change ratio of the divergence angles β_3/β_1 is 0.21, the initial divergence angle is reduced to 1/5, and the particles pass through the nozzle with a particle beam radius within 0.15 mm. In the case of particles measuring 10 μm, γ_3/γ_1 is 0.60, the initial divergence angle is still reduced to 3/5, and the particles safely pass through the nozzle with a particle beam radius within 0.35 mm. It should be emphasized that all values of β and γ keep decreasing along the orifices, implying the successive reduction of the divergence of the particle beam. This clearly demonstrates how the second part of the aerodynamic lens works.

The trajectories of particles with different sizes were all simulated by diversifying the incidence position in the radial direction at the aerodynamic lens inlet. Trajectories of 30-nm particles are simulated with and without Brownian diffusion effect, though the effect has often been neglected for 30-nm particles (Lee et al. 2008, 2009). But the results show a somewhat distinct effect of Brownian diffusion: a measurable difference in the particle trajectories and the resultant beam radius possibly caused by longer residence time. As for 300-nm particles, the Brownian effect was discovered to be insignificant, leading us to neglect the effect for larger particles than 300 nm. The beam radii of particles with different sizes are calculated 40 mm downstream the nozzle exit, in a way that 90% of the total particle flux are enclosed, and shown as a function of particle size in Figure 7a. The results are compared with the results of simulations in previous research conducted by Zhang et al. (2004) and Lee et al. (2008). When taking the diffusion effect into consideration, 30-nm particles reveals an average beam radius of 1.15 mm and, in the 100 nm-2.5 μm range, the particle beam radius was approximately 0.1 mm, thus exhibiting an outstanding focusing ability. The beam radius reached 0.48 mm for 3-μm particles and 0.65 mm, the maximal value, for 4-μm particles, respectively. As the particle diameter increases, the particle beam radius decreases due to inertial impact loss at the edge of the particle beams, and the beam radius of particles measuring 10 μm once again decreases somewhat, reaching 0.53 mm. Overall, the present aerodynamic lens working in a much wider size range could produce either narrower or similar collimated particle beams as compared to our previous lens (Lee et al. 2008) and Zhang et al.'s lens.

In Figure 7b, the transmission efficiency of the present study was compared with the results of previous researches by Liu et al. (2007), Jayne et al. (2000) and Zhang et al. (2004). Particle transmission efficiency amounted to 94% or above for 30 nm–3 μm particles and to 80% or above for 10-μm particles, respectively, thus exhibiting quite an excellent transmission efficiency. Hence, it is clear that such a wide operation range has never been achieved before. As shown in Figure 7a, at particle sizes of 3–10 μm, the particle beam radii of the aerodynamic

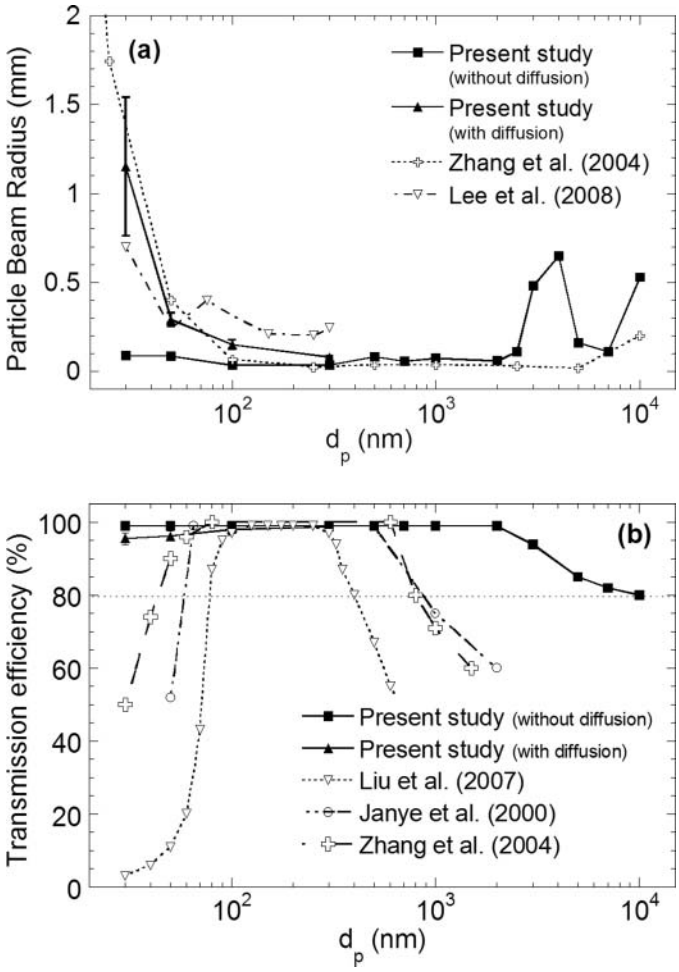

FIG. 7. Performance of the current design of the aerodynamic lens system: (a) beam radius; (b) transmission efficiency of particles as a function of their size.

lenses in Zhang et al. (2004) seem smaller than those in the present study. However, it must be stated that, as shown in Figure 7b, when the particle sizes exceed 600 nm, inertial loss develops suddenly so that the particle beams seem focused due to their cut-off.

4. CONCLUSION

Due to inertial impact loss brought about by the large St of particles, existing aerodynamic lenses were limited in that the range of focusable particle size is just as large as one order of magnitude. How to enlarge the focusable size range to two orders of magnitude (30–3000 nm), or even more, has become the purpose of this study. We demonstrated that the particles' inertial impact could differ significantly depending on their initial incidence position in the radial direction, and that the degree of divergence of particles could be controlled in the orifices flow. Using these results, a new type of aerodynamic lens system were designed by arranging the lenses in such a way that their diameters increased after decreasing first. As a result, in the first

stage, the incidence position of large particles was made to move close to the central axes of the lenses and, in the second stage, the divergence angles of particles were reduced to minimize further inertial impaction. Consequently, such a design minimizes the inertial impact loss of particles with a large St, thus enabling to focus spherical particles measuring 30 nm–10 μm at a high transmission efficiency of 80% or above and with the particle beam radii within ~0.5 mm. Again, it has to be clarified that the present achievement was obtained for the aerodynamic lens alone excluding the critical orifice where micron particles are often lost significantly. A new approach for reducing those losses will be discussed in a forthcoming manuscript.

REFERENCES

Chen, D. R., and Pui, Y. H. (1995). Numerical and Experimental Studies of Particle Deposition in a Tube with a Conical Contraction-Laminar Flow Regime. *J. Aerosol Sci.*, 26:563–574.

Das, R., and Phares, D. J. (2004). Expansion of an Ultrafine Aerosol Through a Thin-Plate Orifice, *J. Aerosol Sci.,* 35:1091–1103.

Deng, R., Zhang, X., Smith, K. A., Wormhoudt, J., Lewis, D. K., and Freedman, A. (2008). Focusing Particle with Diameters of 1 to 10 Microns into Beams at Atmospheric Pressure. *Aerosol Sci. Technol.,* 42:899–915.

Dong. Y., Bapat, A., Hilchie, S., Kortshagen, U., and Campbell, S. A. (2004). Generation of Nano-Sized Free Standing Single Crystal Silicon Particles. *J. Vac. Sci. Technol. B: Microelectron. Nanometer Struct.,* 22:1923–1930.

Fonzo, F. D., Gidwani, A., Fan, M. H., Neumann, D., Iordanoglou, D. I., Heberlein, J. V. R., et al. (2000). Focused Nanoparticle-Beam Deposition of Patterned Microstructures. *Appl. Phys. Lett.,* 77:910–912.

Harris, W. A., Reilly, P. T. A., and Whitten, W. B. (2006). Aerosol MALDI of Peptides and Proteins in an Ion Trap Mass Spectrometer: Trapping, Resolution and Signal-to-Noise. *Int. J. Mass Spectrom.,* 258:113–119.

Jayne, J. T., Leard, D. C., Zhang, X., Davidovits, P., Smith, K. A., Kolb, C. E., et al. (2000). Development of an Aerosol Mass Spectrometer for Size and Composition Analysis of Submicron Particles. *Aerosol Sci. Technol.,* 33:49–70.

Lee, K. S., Cho, S. W., and Lee, D. (2008). Development and Experimental Evaluation of Aerodynamic Lens as an Aerosol Inlet of Single Mass Spectrometry. *J. Aerosol Sci.,* 39:287–304.

Lee, K. S., Kim, S., and Lee, D. (2009). Aerodynamic Focusing of 5–50 nm Nanoparticles in Air. *J. Aerosol Sci.,* 40:1010–1018.

Lee, D., Miller, A., Kittelson, D., and Zachariah, M. R. (2006). Characterization of Metal-Bearing Diesel Nanoparticles Using Single Particle Mass Spectrometry. *J. Aerosol Sci.,* 37:88–110.

Lee, D., Park, K., and Zachariah, M. R. (2005). Determination of Size Distribution of Polydisperse Nanoparticles with Single Particle Mass Spectrometry: The Role of Ion Kinetic Energy. *Aerosol Sci. Technol.,* 39:162–169.

Li, A., and Ahmadi, G. (1992). Dispersion and Deposition of Spherical Particles from Point Sources in a Turbulent Channel Flow. *Aerosol Sci. Technol.,* 16(4):209–226.

Liu, P. S. K., Deng, R., Smith, K. A., Williams, L. R., Jayne, J. T., Canagaratna, M. R., Moore, K., Onasch, T. B., Worsnop, D. R., and Deshler, T. (2007). Transmission Efficiency of an Aerodynamic Focusing Lens System: Comparison of Model Calculations and Laboratory Measurement for the Aerodyne Aerosol Mass Spectrometer. *Aerosol Sci. Technol.,* 41:721–733.

Liu, P., Ziemann, P. J., Kittelson, D. B., and McMurry, P. H. (1995a). Generation Particle Beams of Controlled Dimensions and Divergence: I. Theory of Particle Motion in Aerodynamic Lenses and Nozzle Expansions. *Aerosol Sci. Technol.,* 22:293–313.

Liu, P., Ziemann, P. J., Kittelson, D. B., and McMurry, P. H. (1995b). Generation Particle Beams of Controlled Dimensions and Divergence: II. Experimental Evaluation of Particle Motion in Aerodynamic Lenses and Nozzle Expansions. *Aerosol Sci. Technol.,* 22:314–324.

Murphy, W. K., and Sears, G. W. (1964). Production of Particulate Beams. *J. Appl. Phys.,* 35:1986–1987.

Qi, L., McMurry, P. H., Norris, D. J., and Girshick, S. L. (2010). Micropattern Deposition of Colloidal Semiconductor Nanocrystals by Aerodynamic Focusing. *Aerosol Sci. Technol.,* 44:55–60.

Schreiner, J., Schild, U., Voigt, C., and Mauersberger, K. (1999). Focusing of Aerosols into a Particle Beam at Pressures from 10 to 150 Torr. *Aerosol Sci. Technol.,* 31:373–382.

Schreiner, J., Voigt, C., Mauersberger, K., McMurry, P. H., and Ziemann, P. J. (1998). Aerodynamic Lens System for Producing Particle Beams at Stratospheric Pressures. *Aerosol Sci. Technol.,* 29:50–56.

TSI (2004). Product Information of Series 3800 Aerosol Time-of-Flight Mass Spectrometers with Aerodynamic Focusing Lens Technology. http://www.tsi.com.

Wang, X., Gidwani, A., Girshick, S. L., and McMurry, P. H. (2005). Aerodynamic Focusing of Nanoparticles: II. Numerical Simulation of Particle Motion Through Aerodynamic Lenses. *Aerosol Sci. Technol.,* 39:624–636.

Wang, X., and McMurry, P. H. (2006). A Design Tool for Aerodynamic Lens Systems. *Aerosol Sci. Technol.,* 40:320–334.

Zhang, X., Smith, K. A., Worsnop, D. R., Jimenez, J., Jayne, J. T., and Kolb, C. E. (2002). A Numerical Characterization of Particle Beam Collimation by an Aerodynamic Lens-Nozzle System: Part I. An Individual Lens or Nozzle. *Aerosol Sci. Technol.,* 36:617–631.

Zhang, X., Smith, K. A., Worsnop, D. R., Jimenez, J. L., Jayne, J. T., Kolb, C. E., et al. (2004). Numerical Characterization of Particle Beam Collimation: Part II Integrated Aerodynamic-Lens-Nozzle System. *Aerosol Sci. Technol.,* 38:619–638.